



Delft University of Technology

Protocol for Reading Out Majorana Vortex Qubits and Testing Non-Abelian Statistics

Liu, Chun Xiao; Liu, Dong E.; Zhang, Fu Chun; Chiu, Ching Kai

DOI

[10.1103/PhysRevApplied.12.054035](https://doi.org/10.1103/PhysRevApplied.12.054035)

Publication date

2019

Document Version

Final published version

Published in

Physical Review Applied

Citation (APA)

Liu, C. X., Liu, D. E., Zhang, F. C., & Chiu, C. K. (2019). Protocol for Reading Out Majorana Vortex Qubits and Testing Non-Abelian Statistics. *Physical Review Applied*, 12(5), Article 054035. <https://doi.org/10.1103/PhysRevApplied.12.054035>

Important note

To cite this publication, please use the final published version (if applicable). Please check the document version above.

Copyright

Other than for strictly personal use, it is not permitted to download, forward or distribute the text or part of it, without the consent of the author(s) and/or copyright holder(s), unless the work is under an open content license such as Creative Commons.

Takedown policy

Please contact us and provide details if you believe this document breaches copyrights. We will remove access to the work immediately and investigate your claim.

Protocol for Reading Out Majorana Vortex Qubits and Testing Non-Abelian Statistics

Chun-Xiao Liu^{1,2,3}, Dong E. Liu,^{4,5} Fu-Chun Zhang,^{1,6,7} and Ching-Kai Chiu^{1,2,*}

¹*Kavli Institute for Theoretical Sciences, University of Chinese Academy of Sciences, Beijing 100190, China*

²*Department of Physics, Condensed Matter Theory Center and Joint Quantum Institute, University of Maryland, College Park, Maryland 20742, USA*


³*QuTech and Kavli Institute of Nanoscience, Delft University of Technology, P.O. Box 4056, 2600 GA Delft, The Netherlands*

⁴*State Key Laboratory of Low-Dimensional Quantum Physics and Department of Physics, Tsinghua University, Beijing 100084, China*

⁵*Frontier Science Center for Quantum Information, Beijing 100184, China*

⁶*CAS Center for Excellence in Topological Quantum Computation, University of Chinese Academy of Science, Beijing 100190, China*

⁷*Collaborative Innovation Center of Advanced Microstructures, Nanjing University, Nanjing 210093, China*

 (Received 11 February 2019; revised manuscript received 16 July 2019; published 14 November 2019)

The successful testing of non-Abelian statistics not only serves as a milestone in fundamental physics but also provides a quantum-gate operation in topological quantum computation. An accurate and efficient readout scheme of a topological qubit is an essential step toward the experimental confirmation of non-Abelian statistics. In the current work, we propose a protocol to read out the quantum state of a Majorana vortex qubit on a topological superconductor island. The protocol consists of four Majorana zero modes trapped in spatially well-separated vortex cores on the two-dimensional surface of a Coulomb blockaded topological superconductor. Our proposed measurement is implemented by a pair of weakly coupled Majorana modes separately in touch with two normal-metal leads and the readout is realized by observing the conductance-peak location in terms of the gate voltage. Using this protocol, we can further test the non-Abelian statistics of Majorana zero modes in the two-dimensional platform. A successful readout of a Majorana qubit is a crucial step toward the future application of topological quantum computation. In addition, this Coulomb-blockaded setup can distinguish Majorana zero modes from Caroli–de Gennes–Matricon modes in vortex cores.

DOI: [10.1103/PhysRevApplied.12.054035](https://doi.org/10.1103/PhysRevApplied.12.054035)

I. INTRODUCTION

Majorana zero modes (MZMs) [1,2] are zero-energy quasiparticle excitations with neutral charge in the defects of the topological superconductors (TSCs) [3–14]. A pair of spatially separated MZMs forms a fermionic state, the number occupancy of which encodes the quantum information nonlocally. Such information is robust against most local perturbations and thereby is expected to possess a much longer coherence time [15]. Moreover, MZMs are non-Abelian anyons, i.e., an exchange of two MZMs will rotate the quantum state in the degenerate subspace [15,16]. Thus, quantum gates can be implemented by braid operations. Due to these two properties (nonlocal quantum information storage and non-Abelian statistics), MZMs are a promising candidate for the realization of topological quantum computation.

Following multiple seminal theoretical proposals [17–21], much experimental progress has been made in the realization and detection of MZMs within the context of both one-dimensional [22–32] and two-dimensional (2D) platforms [33–40]. Regarding the 2D case, an *s*-wave superconducting surface with a single Dirac cone, forming an equivalent 2D $p \pm ip$ superconductor, is able to host an MZM emerging in the vortex core [17]. The first candidate of this kind is the heterostructure of the topological insulator (Bi_2Te_3) and the *s*-wave superconductor (NbSe_2). The superconducting proximity effect induces an *s*-wave SC pairing on the surface of the topological insulator. Recent scanning-tunneling-spectroscopy (STS) measurements on $\text{Bi}_2\text{Se}_3/\text{NbSe}_2$ have observed spin-polarization-dependent zero-bias conductance peaks in the vortex cores of the heterostructure [33,34], which are consistent with the MZM interpretation in tunnel spectroscopy [41,42]. However, a major practical problem is that other low-energy modes, e.g., Caroli–de Gennes–Matricon (CdGM) modes, are very

* qiujingkai@ucas.edu.cn

close to the zero mode, so that they cannot be distinguished from the MZM [43]. Recently, experiments on iron-based superconductors ($\text{FeTe}_x\text{Se}_{1-x}$, $\text{Li}_{1-x}\text{Fe}_x\text{OHFeSe}$) have provided more evidence for the possible existence of MZMs in 2D systems, since the level spacing of those CdGM modes is larger than the STS resolution [35–38]. In addition, it has been experimentally observed [44,45] that the tunneling conductance plateaus in the vortex cores are close to $2e^2/h$ at zero bias voltage. Given such encouraging experimental progress made in the detection of MZMs in vortex cores, naturally, the next milestone will be the readout of the quantum information encoded in MZMs. However, so far, most of the experimental efforts are focusing on the Majorana resonance [41], which does not acquire encoded quantum-state information. In addition, practical theoretical proposals for reading out MZMs in 2D TSCs are still elusive, which limits the potential of demonstrating non-Abelian statistics stemming from MZMs in 2D systems.

In this work, we propose a theoretical scheme for reading out a Majorana vortex qubit (MVQ) and testing non-Abelian statistics. The MVQ consists of four MZMs trapped in spatially well-separated vortex cores on the 2D surface of a TSC island with finite charging energy, which could lead to Fu’s Majorana teleportation [46]. Our proposed setup, which is distinct from Fu’s proposal, does not require a loop-geometry coherent channel and a threading flux to achieve electron interference but includes an additional pair of Majorana modes. This island with four MZMs forms a minimum Majorana qubit, removing the extra structural complexity, and therefore is more suitable and feasible for a 2D superconducting island. Interestingly, the electron cotunneling process is identical to that of Fu’s teleportation case. Projective measurement can be implemented by a pair of weakly coupled Majorana modes in touch with separate normal-metal leads in the Coulomb-blockade valley, while high-resolution readout of the measurement outcome can be realized by observing the conductance-peak location at the charge-degenerate points. This readout scheme can be used for braiding readout and further extended to Majorana fusion processes to demonstrate the non-Abelian statistics. The success of reading out a Majorana qubit is a key step toward the future application of topological quantum computation. The rest of the paper is organized as follows. In Sec. II, which is the main part of the work, we introduce the theoretical model of the Majorana vortex qubit and explain how to read out MVQ by a three-step scheme. Section III shows the readout outcome for manifesting the non-Abelian nature of MZMs with the assumption that fusion and braiding operations can be successfully implemented in the TSC island. In Sec. IV, possible experimental methods for moving vortices with MZMs are briefly discussed, with an estimation of the time-scale constraints. In Sec. V, using the same experimental setup, we show how to distinguish

between MZMs and CdGMs through tunnel conductance spectroscopy. Finally, Sec. VI concludes the work with a discussion.

II. READOUT FOR A MAJORANA VORTEX QUBIT

The MVQ is a TSC island hosting four MZMs trapped in spatially separate vortices and the island is capacitively connected to an adjustable external gate, as shown in Fig. 1(a).

The low-energy effective Hamiltonian of the TSC island is as follows:

$$H_C = E_C(N - N_g)^2 + n_{12}E_{12} + n_{34}E_{34}, \quad (1)$$

where $E_C = e^2/C$ is the charging energy, N is the total number of electrons in the TSC island, and $N_g = CV_g/e$ is the induced charge number, which is tunable via the gate voltage (in the following, we use N_g to represent the gate voltage). Among the four MZMs, as shown in Fig. 1(a), γ_1 and γ_2 (γ_3 and γ_4) pair up to form a normal fermionic state with energy E_{12} (E_{34}) and occupancy n_{12} (n_{34}). In the low-energy Hamiltonian of Eq. (1), we assume the hybridizations of the MZMs to be the only relevant excitations, which is true in the low-temperature limit $k_B T \ll \Delta$. The presence of charging energy constrains the Hilbert space: the parity of the total electron number

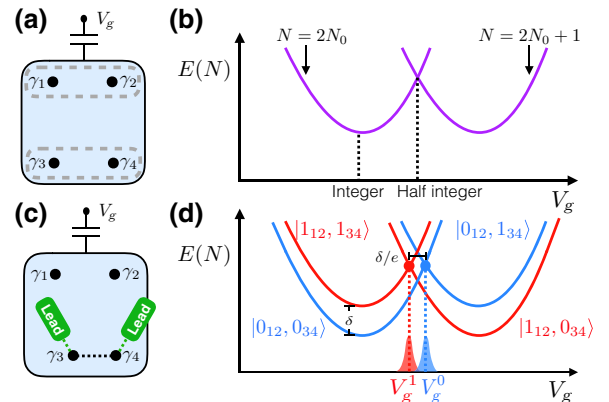


FIG. 1. (a) A schematic of a Majorana qubit. The Majorana qubit is a TSC island, which hosts four spatially separate MZMs and is capacitively connected to an adjustable external gate. The dashed lines indicate the pairing of the MZMs. (b) The energy spectrum of the TSC island as a function of the gate voltage V_g . Each parabola corresponds to a fixed total electron number. The purple lines represent two-fold degeneracy states. (c) A schematic of the projective measurement. We first move γ_3 closer to γ_4 and then couple the two Majoranas to separate the normal-metal leads. The dashed line in (c) indicates the hybridization of γ_3 and γ_4 . (d) The readout process: depending on the measurement outcome in (c), a conductance peak will show up at either V_g^1 (red peak) or V_g^0 (blue peak).

should be equal to $N \bmod 2 = (n_{12} + n_{34}) \bmod 2$. If the four MZMs are spatially well separated ($E_{12}, E_{34} \rightarrow 0$) and the gate voltage is tuned near an integer point $N_g \approx 2N_0$, as shown in Fig. 1(b), there will be two degenerate ground states in the TSC island: $|2N_0; 0_{12}, 0_{34}\rangle$ and $|2N_0; 1_{12}, 1_{34}\rangle$. These two states span the degenerate subspace of a MVQ. In the Coulomb-blockade valley, the MVQ has protection from the spatially separate MZMs and, in addition, the charging energy can significantly reduce the notorious “quasiparticle poisoning” from the outside environment [47–49].

The readout of an arbitrary MVQ state $|\psi\rangle = a|0_{12}, 0_{34}\rangle + b|1_{12}, 1_{34}\rangle$ requires a sequence of efficient projective measurements to obtain the probabilities $|a|^2$ and $|b|^2$. In our scheme, the projective measurement is implemented by measuring the two-terminal conductance via a pair of weakly coupled Majorana modes on the TSC island. Here, we outline the three-step protocol for a single readout process:

(i) For a TSC island in the Coulomb-blockade valley $N_g \approx 2N_0$, we adiabatically lift the double degeneracy between $|2N_0; 0_{12}, 0_{34}\rangle$ and $|2N_0; 1_{12}, 1_{34}\rangle$ by moving γ_3 closer to γ_4 ($E_{34} > 0$).

(ii) We weakly couple the two Majorana modes γ_3 and γ_4 to separate the normal-metal leads near the vortex cores, as shown in Fig. 1(c). The two-terminal conductance measurement would project the MVQ in one of the basis states after a measurement time $t \sim (\Gamma_L \Gamma_R V / E_C^2)^{-1}$. The tunnel broadening of the MZM is defined as $\Gamma_{L(R)} = 2\pi |t_{L(R)}|^2 \rho$, with ρ being the lead density of states and $t_{L(R)}$ being the coupling strength between the MZM and the left (right) lead. V is the voltage drop between the source and drain leads.

(iii) We tune the gate voltage toward the half-integer point, $N_g \approx 2N_0 + 1/2$. Depending on the measurement outcome in step (ii), a conductance peak will show up at the charge degenerate point either to the left or to the right of the half-integer point [Fig. 1(d)]. This peak location tells us in which basis state the MVQ is projected.

The three steps mentioned above lead to a single readout of a MVQ state. To have a statistical estimate of $|a|^2$ and $|b|^2$, we need to repeat the operation for many times: we prepare the qubit into the same initial state and then perform the readout procedure. Now, we will try to flesh out the three-step protocol.

The goal of step (i) is to lift the double degeneracy between the two ground states $|2N_0; 0_{12}, 0_{34}\rangle$ and $|2N_0; 1_{12}, 1_{34}\rangle$. Initially, the four MZMs are spatially well separated ($E_{12}, E_{34} \rightarrow 0$) and the SC island is in the Coulomb-blockade valley $N_g \approx 2N_0$. We then adiabatically move γ_3 closer to γ_4 , while still keeping $\gamma_{1,2}$ far away from each other and from $\gamma_{3,4}$. More details of the vortex

movement will be discussed in Sec. IV. Due to the wavefunction overlap between γ_3 and γ_4 , the coupling between the two modes becomes finite [50,51]:

$$E_{34} \approx \frac{\cos(p_F R_{34} + \pi/4)}{\sqrt{p_F R_{34}}} \exp(-R_{34}/\xi), \quad (2)$$

in the large-distance limit $R_{34} \gg \xi$. Here, R_{34} is the inter-vortex distance between γ_3 and γ_4 , ξ is the SC coherence length, and p_F is the Fermi momentum of the surface Dirac cone. In the limit of $p_F \rightarrow 0$, the energy does not oscillate and we can safely assume $E_{34} = \delta > 0$ to hold when we adjust R_{34} . Now the energies of the two lowest eigenstates are split: $E(2N_0; 1_{12}, 1_{34}) - E(2N_0; 0_{12}, 0_{34}) = \delta$ and this positive energy splitting is crucial to the readout measurement in step (iii). We emphasize that the energy splitting cannot lead to any parity change of the fermion state of $\gamma_{3,4}$, since the fermion parity in the entire system is protected by the charge energy and $\gamma_{3,4}$ do not couple to well-separated γ_1 and γ_2 .

In step (ii), we perform a projective measurement on the MVQ state by a two-terminal conductance measurement in the Coulomb-blockade valley. We weakly couple the Majorana modes $\gamma_{3,4}$ to separate the normal-metal leads. This can be realized by two normal electrodes, two scanning-tunneling-microscopy (STM) tips, or one electrode and one tip [52–57]. For the STM tip, the tunneling strength between the tip and the Majorana modes inside the vortex cores is determined by the spatial separation between the tip and the vortex core. For the normal-electrode case, a dielectric layer needs to be placed between the normal electrode and the vortex core. The corresponding tunneling Hamiltonian is as follows [46]:

$$H_T \approx -t_L d_L \gamma_3 e^{i\phi/2} - t_R d_R \gamma_4 e^{i\phi/2} + \text{H.c.}, \quad (3)$$

where $t_{L(R)}$ is the effective coupling between the left (right) lead and Majorana $\gamma_{3(4)}$, $d_{L(R)}$ annihilates one electron in the left (right) lead, and $e^{i\phi/2}$ increases the number of electrons in the SC island by one. For the SC island in the Coulomb-blockade valley ($N_g \approx 2N_0$), the dominant process for the electron tunneling between the source-drain leads is the single electron cotunneling process, which is a second-order process in terms of the tunneling Hamiltonian:

$$\begin{aligned} H_{\text{co}} &= \sum_m \frac{\langle 2N_0; n_{34} | H_T | m \rangle \langle m | H_T | 2N_0; n_{34} \rangle}{E(m) - E(2N_0; n_{34})} \\ &\approx \frac{-2it_L t_R^*}{E_C} \left[\frac{2n_{34} - 1}{1 - 4(\Delta N)^2} + \frac{\delta}{E_C} \frac{1 + 4(\Delta N)^2}{[1 - 4(\Delta N)^2]^2} \right] \\ &\quad d_R^\dagger d_L + \text{H.c.}, \end{aligned} \quad (4)$$

where $\Delta N = N_g - 2N_0$, and $|m\rangle$ is a virtual state with total number of electrons $m = 2N_0 \pm 1$. The leading-order

term in the cotunneling transmission amplitude has a π phase shift depending on the occupancy n_{34} , while the next-order correction is a constant of order $O(\delta/E_C)$. During the whole process, n_{12} is safely protected by the large Majorana separation. Note that Eq. (4) is equivalent to the transmission Hamiltonian derived in Refs. [46] and [47], but instead of a loop-geometry coherent channel and a threading flux used for nanowire systems with two Majorana modes, here we use four Majorana modes to achieve the same coherent electron transport. The elimination of a loop geometry makes our proposal more feasible for a 2D superconducting island. Now we turn on a small bias voltage between the two leads. After a sufficiently long time $t > (\Gamma_L \Gamma_R V/E_C^2)^{-1}$, an electric current flows through γ_1 and γ_2 so that the conductance measurement becomes projective, i.e., the MVQ state $|\psi\rangle = a|0_{12}, 0_{34}\rangle + b|1_{12}, 1_{34}\rangle$ will collapse into either $|0_{12}, 0_{34}\rangle$, with probability $|a|^2$, or $|1_{12}, 1_{34}\rangle$, with probability $|b|^2 = 1 - |a|^2$ [47]. However, the difference between the conductance magnitudes for the two basis states with $n_{34} = 0$ or 1 is tiny and is of order $O(\delta/E_C)$, as shown in Eq. (4). Thereby, even though the MVQ is projected into one of the basis states, it is hard to tell which one by merely observing the magnitude of the cotunneling conductance.

Naturally, the goal of step (iii) is to read out the outcome of the projective measurement in a more transparent way. The key is to tune the gate voltage close to the half-integer point $N_g \approx 2N_0 + 1/2$, which is near the charge-degenerate point. At the charge-degenerate point of the two states with the same n_{12} occupancy, a conductance peak arises because an electron can freely tunnel in and out of the Majorana modes γ_3 and γ_4 without costing additional energy. The reason for fixed n_{12} in the projected state is that isolated γ_1 and γ_2 are always topologically protected. Due to the energy splitting introduced in step (i), as shown in Fig. 1(d), the charge-degenerate point for $|2N_0; 0_{12}, 0_{34}\rangle$ and $|2N_0 + 1; 0_{12}, 1_{34}\rangle$ is shifted to the right of the half-integer point (blue dot), located at $N_g^0 = 2N_0 + 1/2 + \delta/2E_C$, while that for $|2N_0; 1_{12}, 1_{34}\rangle$ and $|2N_0 + 1; 1_{12}, 0_{34}\rangle$ is shifted to the left of the half-integer point (red dot), located at $N_g^1 = 2N_0 + 1/2 - \delta/2E_C$. Therefore, after the MVQ is projected in $|0_{12}, 0_{34}\rangle$ ($|1_{12}, 1_{34}\rangle$) in the Coulomb-blockade valley, as we tune the gate voltage toward the half-integer point, a blue (red) peak will show up at V_g^0 (V_g^1). In other words, observing the conductance-peak location in the gate voltage completes the readout of a MVQ. Furthermore, in order to have high resolution in the readout measurement, the tunneling and thermal broadening need to be less than the conductance-peak separation ($\Gamma, k_B T < \delta$).

On the other hand, the three-step protocol could serve as the initialization of a qubit. Once the target initialized state is confirmed by the conductance-peak location, we tune the gate voltage back to the Coulomb-blockade valley, remove the normal-metal leads, and separate the two Majorana

vortices. Consequently, this qubit state is initialized and ready for quantum information processing.

III. TESTING THE NON-ABELIAN NATURE OF MAJORANA ZERO MODES

We now briefly discuss two proposals for testing the non-Abelian nature of MZMs—one through the fusion process and the other through the braiding process. We emphasize that our focus is still on the readout of the final quantum states, assuming that the fusion and braiding processes can be successfully implemented. A detailed discussion of the experimental realization of fusing and braiding MZMs is beyond the scope of the current work. The schematic of the fusion proposal is shown in Fig. 2(a). Initially, four MZMs are spatially nearby and couple to each other and the system equilibrates to the unique ground state. In the upper path, we adiabatically separate $\gamma_{1,2}$ from $\gamma_{3,4}$ and then move each MZM away from the other to suppress any MZM hybridization. This gives the final state $|0_{12}, 0_{34}\rangle$, since in the intermediate step, n_{12} and n_{34} are good quantum numbers. In the lower path, however, starting from the same initial state, we first separate $\gamma_{1,3}$ from $\gamma_{2,4}$ and then move each MZM away from the other. For the same reason, the corresponding final state would be $|0_{13}, 0_{24}\rangle = (1/\sqrt{2})(|0_{12}, 0_{34}\rangle - i|1_{12}, 1_{34}\rangle)$. We thus see that two procedures to create MZMs in the vacuum lead to two different final states, which provides a direct demonstration of the non-Abelian fusion of MZMs

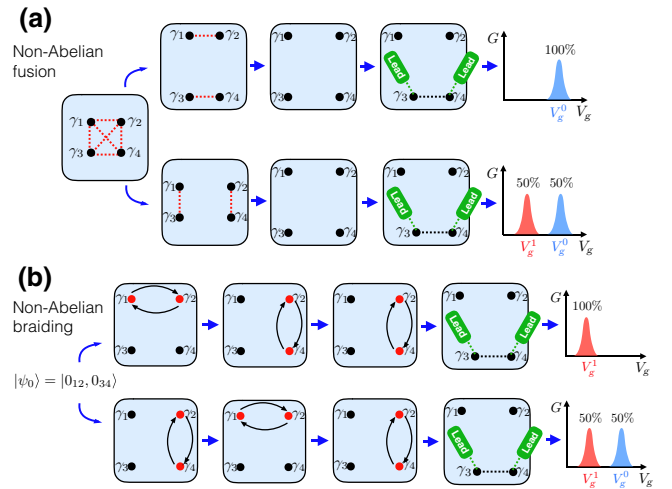


FIG. 2. (a) The proposal for testing the non-Abelian fusion of MZMs. Initially, all the four Majoranas are coupled with each other. The upper and lower paths correspond to different ways of adiabatically decoupling the Majoranas, leading to different final states. (b) The proposal for testing the non-Abelian braiding of MZMs. Starting from the same initial state $|0_{12}, 0_{34}\rangle$, the qubit system is then applied by the same set of braid operations but in a different order. The final states corresponding to the two orders are distinct.

[3]. The distinction between the two final states can be revealed by the conductance-peak locations in our readout protocol—the upper path results in a peak only located at V_g^0 , while the lower one leads to a peak located at V_g^0 or V_g^1 , with equal probability. On the other hand, the schematic for the non-Abelian braiding process is shown in Fig. 2(b). Suppose that the MVQ is initialized in state $|0_{12}, 0_{34}\rangle$ and braid operation has been experimentally achieved. In the upper path, after we adiabatically exchange $\gamma_{1,2}$ and then exchange for twice $\gamma_{2,4}$, the final state is given by $-e^{-i\pi/4}|1_{12}, 1_{34}\rangle$. In the lower path, however, starting from the same initial state, we first exchange $\gamma_{2,4}$, then $\gamma_{1,2}$, and then $\gamma_{2,4}$ again. The resulting final state is $(-i/\sqrt{2})(|0_{12}, 0_{34}\rangle - i|1_{12}, 1_{34}\rangle)$. The same set of braid operations, which is applied on the same initial state in a different order, leads to two distinct final states. This thereby demonstrates the non-Abelian braiding of MZMs. Similar to the fusion process, this distinction between two final states can be revealed by the location of the conductance peaks in our readout protocol.

IV. MOVING VORTICES WITH MZMs

Eventually, the readout of the MVQ requires tuning of the mutual Majorana coupling strengths. The straightforward way to achieve this coupling adjustment is to meticulously move vortices with MZMs. Although precisely controlling the locations of the vortices is a difficult task, it is encouraging that experimentalists have been able to control the locations of the vortices by using magnetic force microscopy in a thin film of superconducting niobium [58]. A recent proposal extends this technique to manipulate vortices in $\text{FeTe}_x\text{Se}_{1-x}$ [59]. This holds out the promise that controlling vortices with MZMs can be achieved in the near future.

$\text{FeTe}_x\text{Se}_{1-x}$ is one of the ideal platforms hosting MZMs in vortex cores. We use $\text{FeTe}_x\text{Se}_{1-x}$ with real physical parameters as an example to provide a practical recipe for vortex movement without poisoning the MVQ before the MVQ readout. We adapt the simulation program in Ref. [60], which faithfully describes the Majorana physics on the surface of $\text{FeTe}_x\text{Se}_{1-x}$. At the beginning of the MVQ readout, we keep four MZMs residing in four separate vortices far apart, with an intervortex distance of roughly 100 nm so that their suppressed hybridization protects the MVQ. To achieve the readout, we bring one of the vortices (γ_3) close to another (γ_4), as illustrated in Fig. 1(c). Since the hybridization energy ΔE is on the order of $0.1 \mu\text{eV}$ in the simulation, we expect that the time scale to move the vortex should be short enough ($\tau \ll \hbar/\Delta E = 7 \text{ ns}$) so that the Majorana hybridization does not poison the MVQ. On the other hand, the lowest energy (Δ^2/E_F) of the CdGM modes is close to the Majorana splitting $\delta = 0.2 \text{ meV}$ [37,60–62]. The time scale of the Majorana movement should be long enough ($\tau \gg$

$\hbar/\Delta^2/E_F = 3 \text{ ps}$) so that the MZMs cannot be excited to the CdGM states. On the other hand, since, currently, the best energy resolution of STM is around $20 \mu\text{eV}$ [63], to have detectable energy splitting we suggest that the distance between the two hybridized MZMs should be 40 nm, based on the Majorana-physics simulation in $\text{FeTe}_x\text{Se}_{1-x}$ [60]. Fortunately, 40 nm is an experimentally reachable distance between the STM tips, since two tips 72 nm apart have already been made successfully in the laboratory [57]. For the readout, adjusting the Majorana distance from 100 nm to 40 nm is much more accessible than physically braiding two Majorana modes, since the braiding leads to twisted vortex lines in the bulk. We emphasize that this energy splitting does not affect the time scale of the vortex movement, since the charge energy can protect the fermion parity of the two isolated hybridized MZMs (γ_1 and γ_2). This is the main idea of our proposal, by using the protection of the charge energy.

The non-Abelian fusion that we propose can be achieved by using similar length and time scales. For the non-Abelian braiding, the time scale of MZM exchange is similarly in the time region of the readout. Alternatively, without exchanging the positions of the vortex cores, the exchange of Majorana modes can also be implemented through three successive projective measurements [64,65].

V. CAROLI–DE GENNES–MATRICON MODES

CdGM modes with low energy always coexist with a MZM in a vortex core [43]. As we will show, near the charge-energy-degenerate point, the readout measurement through resonant tunneling not only accurately reads out the MVQ but also clearly distinguishes MZMs from CdGM modes when the temperature is very close to the energy of the CdGM modes.

We first consider the case in which the two vortex cores in contact with the leads possess only two CdGM modes separately, with energies E_1 and E_2 , where $E_1 \lesssim E_2$. When these two vortices are spatially close, the overlapping of the two CdGM modes leads to the gate-voltage (V_g) location of the conductance peak near E_1 and E_2 referenced to the half-integer point, since the CdGM modes effectively become extended states [66]. At $k_B T \sim E_1, E_2$, as the intervortex distance increases, as shown in Fig. 3(a) the conductance monotonically decreases and the V_g location of the conductance peak moves to the half-integer point [67], which is identical to the case in the presence of the MZMs, as shown in Fig. 3(b). On the other hand, consider that each vortex possesses a MZM and one of the two vortices has a CdGM mode with energy $E_1 > 0$. At any temperature, as shown in Fig. 3(b) the gate voltage of the conductance peak is fixed at zero due to the strong electron cotunneling assisted by the MZMs [46]. For $k_B T \sim E_1$, the CdGM mode contributes a small portion of the conductance peak in the short intervortex distance. As the

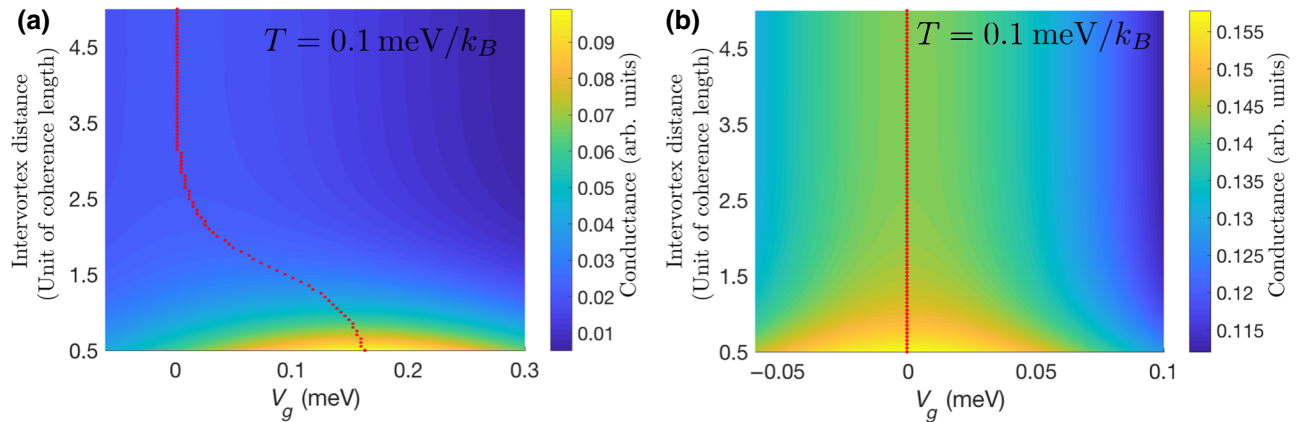


FIG. 3. The conductance for MZMs and CdGM modes as a function of the gate voltage and the intervortex distance. Here, $V_g = 0$ corresponds to the half-integer point $N_g = 2N_0 + 1/2$ and the coherence length of the MZMs and the CdGM modes is chosen to be unity. (a) The conductance for two separated CdGM modes of energies 0.2 and 0.21 meV in the absence of MZMs. At $k_B T \approx 0.2$ meV, the conductance-peak location (red dashed line) shifts from $V_g \approx 0.16$ mV to 0 mV as the intervortex distance increases. (b) The conductance for two MZMs in two separate vortex cores, with a single CdGM mode of energy 0.2 meV inside one of the vortices. The conductance peak always appears at $V_g = 0$ mV.

intervortex distance increases, the conductance from the CdGM contribution is suppressed.

Thus, the key to distinguishing the MZM from the CdGM mode is that at the temperature comparable to the energy of the CdGM mode, the conductance-peak location stays (varies) in the presence (absence) of MZMs as the intervortex distance increases.

VI. SUMMARY AND DISCUSSION

Strong clues concerning a single MZM bounded in a vortex core of a TSC have been revealed by recent experiments [35–38]. Taking advantage of this important progress, we propose a feasible protocol for reading out the quantum information encoded in the vortex MZMs by using the well-developed Coulomb-blockade transport measurement [29]. We expect the size of the $\text{FeTe}_x\text{Se}_{1-x}$ island to be close to the London penetration depth (approximately 500 nm) [68,69] to host a few MZMs; hence, this small island leads to large charging energy (< 2.9 meV), which is greater than the experimental temperature, thus protecting the MVQ. This is encouraging given that similar superconducting islands hosting a few vortices have been made in the laboratory [70]. Since the readout of the MVQ always requires the hybridization of the two MZMs, the quantum information of the original qubit might be lost due to quasiparticle poisoning and relaxation to the ground state. The two isolated MZMs $\gamma_{1,2}$ and the Coulomb-blockaded superconductor with a large charging energy protect the MVQ during the readout progress. The true value of the tunneling conductance, which in reality is commonly affected by unknown factors, is difficult to be a suitable observable to determine the quantum state.

To circumvent this problem, we show that the V_g location of the conductance peak can determine the eigenstate of the MVQ. This is the key idea of our readout protocol—regardless of the precise conductance value, measurement of the V_g location of the conductance peak is more experimentally feasible in principle; this can be compared to the original Aharonov-Bohm interferometer [46], which requires strong coherence and an extra metallic arm in the device. Furthermore, the extension of this readout protocol can be applied to Majorana qubits in nanowire setups [47,48].

The tunneling of the Coulomb-blockaded island can further confirm the presence of MZMs with the coexistence of the CdGM modes. At temperatures comparable to the energy of the CdGM modes, the gate-voltage location of the peak conductance is again an important observable to distinguish the MZMs from the CdGM modes. Confirmation of the existence of MZMs in the vortices is the primary step to experimentally achieve our readout protocol.

Another important implementation of the Coulomb-blockade design is the initialization of the quantum state protected by the charging energy. Using this initialization, we create multiple identical quantum states (disregarding the phase difference) to statistically test the non-Abelian statistics. An experimental demonstration of the Majorana non-Abelian statistics is a milestone toward topological quantum computation. Hopefully, our proposal paves the way toward reaching this goal.

ACKNOWLEDGMENTS

We thank H. Ding, M. Franz, D. L. Feng, T. Hanaguri, T. Y. Liu, J. Jia, L. Y. Kong, D. F. Wang, T. Machida,

S. Das Sarma, R. Wiesendanger, H. Zhang, and H. Zheng for fruitful discussions. C.-X.L. and C.-K.C. acknowledge the support from the Laboratory for Physical Sciences and Microsoft. C.-X. L. is supported by a subsidy for top consortia for knowledge and innovation (TK1 toeslag) by the Dutch ministry of economic affairs. C.-K.C. and F.-C.Z. are supported by the Strategic Priority Research Program of the Chinese Academy of Sciences (Grant No. XDB28000000). D.E.L. is supported by the State Key Laboratory of Low-Dimensional Quantum Physics at Tsinghua University. F.-C.Z. is also supported by the National Science Foundation of China (Grant No. NSFC-11674278).

APPENDIX A: DERIVATION OF COTUNNELING HAMILTONIAN

Here, we derive the low-energy Hamiltonian for the single-electron cotunneling process between two normal-metal leads. The Majorana modes $\gamma_{3,4}$ inside the vortex cores of the SC island are weakly coupled to each other, possibly due to wave-function overlap, and in addition we weakly couple $\gamma_{3,4}$ with separate normal-metal leads. The corresponding Hamiltonian is as follows:

$$H_{\text{SC}} = E_C(N - N_g)^2 + n_{34}\delta,$$

$$H_{\text{leads}} = \sum_{\alpha=L/R,k} \xi_{\alpha,k} c_{\alpha,k}^\dagger c_{\alpha,k},$$

$$H_T = -t_L d_L \gamma_3 e^{i\phi/2} - t_R d_R \gamma_4 e^{i\phi/2} + \text{H.c.}, \quad (\text{A1})$$

where H_{SC} is the Hamiltonian of the TSC island with total electron number N and charging energy E_C , N_g is the gate electron number, δ is the strength of the coupling between γ_3 and γ_4 , and n_{34} the occupation number of the normal fermion state composed by γ_3 and γ_4 . H_{leads} is the Hamiltonian of the two separate normal-metal leads, $c_{\alpha,k}$ is the electron in lead α , and $\xi_{\alpha,k}$ is the occupation energy. $d_\alpha = \sum_k c_{\alpha,k}$ is the electron at the contact point with the vortex in the TSC island. H_T is the coupling Hamiltonian between the lead electrons and the Majorana modes inside the vortex core. t_α is the effective coupling strength between the lead electron and the Majorana mode and $e^{i\phi/2}$ increases the total number of electrons inside the SC island by one. We assume that the gate voltage is tuned in the Coulomb-blockade valley ($N_g \approx 2N_0$) such that the transmission of electrons through the island is dominated by a second-order process. Here, we only consider the transmission process of an electron tunneling from the left lead to the right lead (the opposite process from right to the left lead is simply the Hermitian conjugate term). For state $|2N_0; 0_{12}, 0_{34}\rangle$, the effective Hamiltonian is as follows:

$$H_{00} = \frac{\langle 2N_0; 00 | -t_R^* d_R^\dagger \gamma_4 e^{-i\phi/2} | 2N_0 + 1; 01 \rangle \langle 2N_0 + 1; 01 | -t_L d_L \gamma_3 e^{i\phi/2} | 2N_0; 00 \rangle}{E(2N_0 + 1; 01) - E(2N_0; 00)}$$

$$+ \frac{\langle 2N_0; 00 | -t_L d_L \gamma_3 e^{i\phi/2} | 2N_0 - 1; 01 \rangle \langle 2N_0 - 1; 01 | -t_R^* d_R^\dagger \gamma_4 e^{-i\phi/2} | 2N_0; 00 \rangle}{E(2N_0 - 1; 01) - E(2N_0; 00)}$$

$$= \frac{-2it_L t_R^* d_R^\dagger d_L}{E_C} \frac{1 + \delta/E_C}{(1 + \delta/E_C)^2 - 4\Delta N^2}, \quad (\text{A2})$$

where $\Delta N = N_g - 2N_0$. Note that the virtual state in the second-order process $|2N_0 \pm 1; 01\rangle$ can hold one more or one less electron with the fermion state by virtue of $\gamma_{3,4}$ being occupied. Similarly, for state $|2N_0; 1_{12}, 1_{34}\rangle$, we will obtain

$$H_{11} = \frac{\langle 2N_0; 11 | -t_R^* d_R^\dagger \gamma_4 e^{-i\phi/2} | 2N_0 + 1; 10 \rangle \langle 2N_0 + 1; 10 | -t_L d_L \gamma_3 e^{i\phi/2} | 2N_0; 11 \rangle}{E(2N_0 + 1; 10) - E(2N_0; 11)}$$

$$+ \frac{\langle 2N_0; 11 | -t_L d_L \gamma_3 e^{i\phi/2} | 2N_0 - 1; 10 \rangle \langle 2N_0 - 1; 10 | -t_R^* d_R^\dagger \gamma_4 e^{-i\phi/2} | 2N_0; 11 \rangle}{E(2N_0 - 1; 10) - E(2N_0; 11)}$$

$$= \frac{2it_L t_R^* d_R^\dagger d_L}{E_C} \frac{1 - \delta/E_C}{(1 - \delta/E_C)^2 - 4\Delta N^2}. \quad (\text{A3})$$

Compared to H_{00} , we note that the virtual state in the second-order process $|2N_0 \pm 1; 10\rangle$ has the fermion state by virtue of $\gamma_{3,4}$ being unoccupied, which explains why $\delta \rightarrow -\delta$. What is more, there is an additional overall factor of -1 relative to H_{00} due to the opposite parity of the ground state. Note that there are no off-diagonal terms such as H_{01} or H_{10} because the ground-state Fermi parity does not change after two single-electron-tunneling events. Thus the cotunneling Hamiltonian including H_{00} and H_{11} is as follows:

$$H_{\text{co}} = \frac{-2it_L t_R^* d_R^\dagger d_L}{E_C} \frac{1 + \delta/E_C S}{(1 + \delta/E_C S)^2 - 4\Delta N^2} S$$

$$\approx \frac{-2it_L t_R^* d_R^\dagger d_L}{E_C} \left(\frac{1}{1 - 4\Delta N^2} S - \frac{\delta}{E_C} \frac{1 + 4\Delta N^2}{(1 - 4\Delta N^2)^2} \right), \quad (\text{A4})$$

where we only keep terms up to $O(\delta/E_C)$ and S is a prefactor with $S = 1$ for $|2N_0; 00\rangle$ and $S = -1$ for $|2N_0; 11\rangle$.

APPENDIX B: FUSION PROCESS FOR FOUR MAJORANA MODES ON A SC ISLAND

For the fusion process, our goal is to show that for four initially mutually coupled Majorana modes, different ways and/or paths of keeping all them apart lead to different ground states. Such a path dependence of the final ground state is a direct demonstration of the non-Abelian nature of MZMs (i.e., Ising anyons). The Hamiltonian for the mutually coupled four Majorana modes on a SC island (shown in Fig. 4) is as follows:

$$H = H_h + H_v + H_d + H_C,$$

$$H_h = it_h(\gamma_1\gamma_2 + \gamma_3\gamma_4) = -2t_h(\tau_z \oplus 0),$$

$$H_v = it_v(\gamma_1\gamma_3 - \gamma_2\gamma_4) = 2t_v(\tau_y \oplus 0),$$

$$H_d = it_d(-\gamma_1\gamma_4 + \gamma_2\gamma_3) = -2t_d(0 \oplus \sigma_x),$$

$$H_C = E_C(0 \oplus \sigma_0). \quad (\text{B1})$$

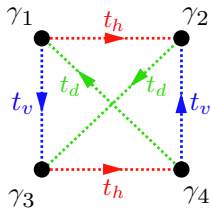


FIG. 4. Four weakly coupled Majorana modes. The coupling amplitude between each pair of Majorana modes is proportional to the strength of the mutual coupling t_{α} and a phase factor $s_{mn} = \pm i$. The sign of the phase factor is constrained by the Z_2 gauge symmetry of the magnetic field and is indicated by the arrow: coupling along the arrow direction gives $s = i$, while coupling opposite to the arrow direction gives $s = -i$.

For each pair of coupled Majorana modes in the form of $st_{mn}\gamma_m\gamma_n$, t_{mn} denotes the strength of the coupling, which we set as a positive value in the low-chemical-potential limit, and $s = \pm i$ is a phase factor constrained by the Z_2 gauge symmetry of the magnetic field [71]. Here, we define $f_1 = (\gamma_1 + i\gamma_2)/2$ and $f_2 = (\gamma_3 + i\gamma_4)/2$ and the Hilbert space is spanned by $(|0\rangle, f_1^\dagger f_2^\dagger |0\rangle, f_1^\dagger |0\rangle, f_2^\dagger |0\rangle)$. Due to the parity symmetry in the coupling Hamiltonian, each term of the coupling Hamiltonian can be diagonalized into two blocks, with even and odd parity, respectively. τ_α ($\alpha = 0, x, y, z$) are Pauli matrices acting on the even-parity subspace spanned by $(|0\rangle, f_1^\dagger f_2^\dagger |0\rangle)$, while σ_α are Pauli matrices acting on the odd-parity subspace spanned by $(f_1^\dagger |0\rangle, f_2^\dagger |0\rangle)$ and 0 is a null matrix. In the strong Coulomb-blockade limit $E_C \gg t_{mn}$, the subspace with odd parity is pushed upward in energy, and we can simply project the total Hamiltonian onto the even-parity subspace in the calculation of the ground state. The projected Hamiltonian and its eigenvalues are as follows:

$$H' = -2t_h\tau_z + 2t_v\tau_y,$$

$$E = \pm 2\sqrt{t_h^2 + t_v^2}. \quad (\text{B2})$$

Initially, when the four Majorana modes are coupled with $t_h = t_v$, the ground state is $|\Psi\rangle \propto (1 + \sqrt{2}, i)$. If we adiabatically turn off the coupling t_v while keeping t_h unchanged, as shown in the upper-path-of-fusion panel in Fig. 2, the ground state will adiabatically evolve into $|\Psi\rangle = (1, 0) = |0\rangle$. On the other hand, if we adiabatically turn off the coupling t_h while keeping t_v unchanged, as shown in the lower-path-of-fusion panel in Fig. 2, the final ground state will be $|\Psi\rangle = (1, -i) \propto |0\rangle - if_1^\dagger f_2^\dagger |0\rangle$. Note that there is no level crossing between the ground state and the first excited state in either of the adiabatic processes, as the level crossing requires all the coefficients of Pauli matrices to vanish, which does not happen in the middle of the adiabatic process that we consider here. Therefore the ground state is uniquely determined. We thus have shown that different ways of separating weakly coupled Majorana modes lead to different final ground states. Although the non-Abelian “separation” process of MZMs is opposite to the “fusion” process, it can equally demonstrate the non-Abelian statistics of MZMs.

APPENDIX C: DISTINGUISHING MZMs FROM CdGM MODES

Measuring the two-terminal conductance of the Coulomb-blockaded superconducting island can provide the readout of the Majorana qubits. Our readout proposal motivates us to check if the location of the conductance peak can differentiate between the MZMs and the CdGM

modes. Hence, we focus on the gate voltage (V_g) near resonant tunneling and use the master equation of the superconducting Coulomb blockade [67] to capture the physics of the weak tunneling. Consider two vortices trapping MZMs or CdGM modes and two lead tips being moved to weakly couple the two vortex cores separately as the two terminals for the tunneling, as shown in Fig. 5. We are interested in two cases: (a) each of the vortices possesses one CdGM mode only and (b) one vortex has one MZM only and the other has one MZM and one CdGM mode. Therefore, the tunneling physics can be effectively described by two

fermions with energy E_i ($i = 1, 2$) and the tunneling rates for these two fermions are labeled by $\Gamma_i^{l,r}$ for particle tunneling in the left (right) vortex and $\Lambda_i^{l,r}$ for hole tunneling in the left (right) vortex. To simplify the problem, we consider the resonant tunneling between the electron numbers N and $N - 1$, where N is even. Since at temperature T in equilibrium, the general form of the conductance for the superconducting island via two low-energy fermions was derived in Ref. [67] [refer to Eqs. (2.26)–(2.30)], we simply use Eq. (2.30) in Ref. [67]:

$$\begin{aligned} \frac{dI}{dV} = & \beta e^2 \left\{ P_{N-1}^{\text{eq}}(0, 1) f(\epsilon_1) \frac{\Gamma_1^l \Gamma_1^r}{\Gamma_1} + P_{N-1}^{\text{eq}}(1, 0) f(\epsilon_2) \frac{\Gamma_2^l \Gamma_2^r}{\Gamma_2} + P_{N-1}^{\text{eq}}(1, 0) f(\tilde{\epsilon}_1) \frac{\Lambda_1^l \Lambda_1^r}{\Lambda_1} + P_{N-1}^{\text{eq}}(0, 1) f(\tilde{\epsilon}_2) \frac{\Lambda_2^l \Lambda_2^r}{\Lambda_2} \right. \\ & - (\gamma_1^l - \gamma_2^l + \lambda_1^l - \lambda_2^l)(\gamma_1^r - \gamma_2^r + \lambda_1^r - \lambda_2^r) \\ & \left. \times \left(\frac{1}{P_{N-1}^{\text{eq}}(0, 1) f(\epsilon_1) \Gamma_1} + \frac{1}{P_{N-1}^{\text{eq}}(1, 0) f(\epsilon_2) \Gamma_2} + \frac{1}{P_{N-1}^{\text{eq}}(1, 0) f(\tilde{\epsilon}_1) \Lambda_1} + \frac{1}{P_{N-1}^{\text{eq}}(0, 1) f(\tilde{\epsilon}_2) \Lambda_2} \right)^{-1} \right\}, \quad (\text{C1}) \end{aligned}$$

where $\Gamma_i = \Gamma_i^l + \Gamma_i^r$, $\Lambda_i = \Lambda_i^l + \Lambda_i^r$, $\gamma_i^\alpha = \Gamma_i^\alpha / \Gamma$, $\lambda_i^\alpha = \Lambda_i^\alpha / \Lambda$ ($\alpha = l, r$), and $\beta = 1/k_B T$. The complicated tunneling formula is determined by various functions, which are the Gibbs distributions $P_{N-1}^{\text{eq}}(1, 0) = e^{-\beta E_1} / Z$, $P_{N-1}^{\text{eq}}(0, 1) = e^{-\beta E_2} / Z$ and the Fermi-Dirac distribution $f(\epsilon) = 1/(1 + e^{\beta \epsilon})$, where $Z = e^{-\beta E_1} + e^{-\beta E_2} + E^{-\beta(E_1 + E_2 + \Delta U)} + e^{-\beta \Delta U}$, $\Delta U = E_c(2N - 2N_g - 1)$, $\epsilon_i = E_i + \Delta U$, $\tilde{\epsilon}_i = -E_i + \Delta U$. Once the physical values of E_1, E_2, T and the tunneling rates are given, the conductance formula is a function of the gate voltage V_g , where $V_g = eN_g/C$. We change the reference of the gate voltage $V_g \rightarrow V_g - [C(2N - 1)]/2e$ so that the charging energies with the electron number $N - 1$ and N are identical ($\Delta U = 0$) at $V_g = 0$, which is the conductance peak of the resonant tunneling via MZMs [72].

(a) While each vortex possesses one CdGM mode, the spatial distribution of the CdGM wave function $\Psi(r)$ can

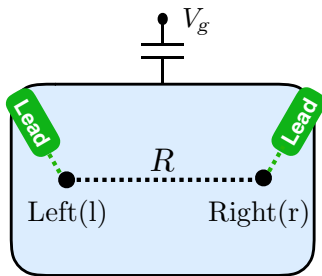


FIG. 5. The two lead tips weakly couple two vortices separately on the surface of the superconductor.

be captured by the Bessel functions [73,74]. With the coherence length ξ of the superconductor, the wave function is approximately proportional to $\Psi(r) \sim e^{-r/\xi}$ with Friedel-like oscillation, the length of which is given by the Fermi wavelength $1/k_F$ from the bulk or the surface band at the Fermi level. Here, we consider $k_F = 0$ so that the wave function exhibits only spatial exponential decay. For the CdGM mode with energy E_1 located at the left vortex, we can assume the tunneling rates $\Gamma_1^l = \Lambda_1^l = 1$ and $\Gamma_1^r = \Lambda_1^r = e^{-2R/\xi}$, where R is the inter-vortex distance; the exponential decay of the tunneling rates in the right vortex core stems from the spatial distribution of the CdGM mode trapped in the left vortex. Similarly, for the CdGM mode with E_2 located at the right vortex, the tunneling rates are given by $\Gamma_2^r = \Lambda_2^r = 1$ and $\Gamma_2^l = \Lambda_2^l = e^{-2R/\xi}$. We note that knowledge of the exact value of the conductance is not required in this case, since it will be shown later that the location of the conductance peak is the main observable to distinguish MZMs and CdGM modes. We choose $E_1 = 0.2$ meV and $E_2 = 0.21$ meV and use Eq. (C1) to compute the conductance at $T = 0.1$ meV $\sim E_1, E_2$ and $T = 0.01$ meV $\ll E_1, E_2$. When these two vortices are spatially close, the overlapping of the two CdGM modes leads to the strong tunneling conductance and the gate voltage (V_g) of the conductance peak is near E_1 and E_2 , since the CdGM modes effectively become extended states [66]. For $k_B T \sim E_1, E_2$, when the distance (R) between the two vortices increases, the conductance monotonically decreases and is close to a nonzero constant and the gate voltage of

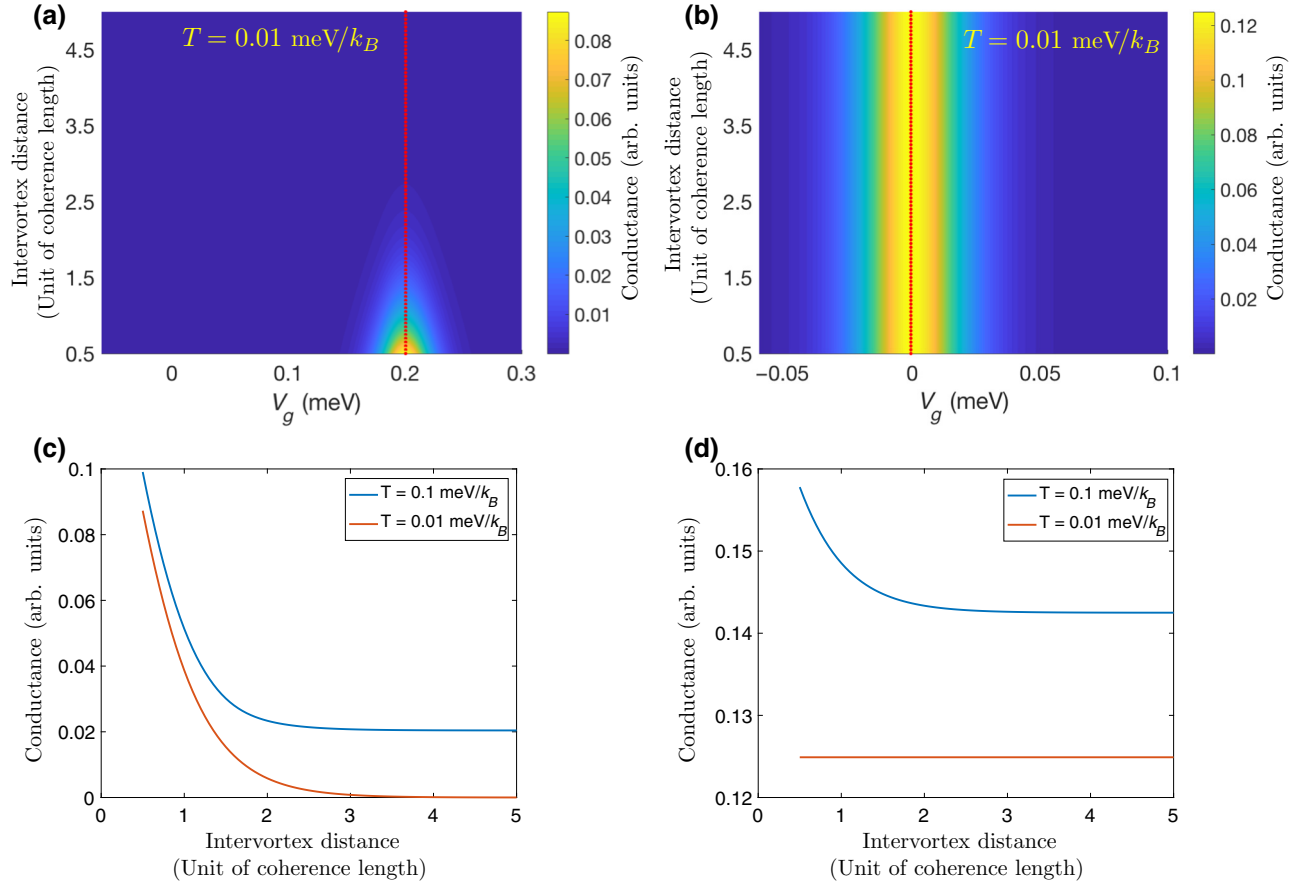


FIG. 6. The tunneling conductance (a),(b) and the conductance peak (c),(d) of the Coulomb-blockaded superconducting island with the two leads in contact with the two vortices, respectively, where $V_g = 0$ corresponds to the resonant point $N_g = N + 1/2$. (a),(c) Two CdGM modes located at two spatially separated vortex cores have energies of 0.2 and 0.21 meV, respectively, without MZMs. Since the red dashed lines in (a),(b) represent the conductance peaks, for $k_B T \ll E_1$, the V_g location of the conductance peak is independent of the intervortex distance. Panel (c) shows that the conductance exponentially decays to zero as a function of the intervortex distance at $k_B T \ll E_1$. (b),(d) Two MZMs are located at two vortices separately and one of the two vortices possesses a CdGM mode with energy 0.2 meV. The conductance mainly stemming from the resonant tunneling via the MZMs is always a nonzero constant at any intervortex distance. For $k_B T \sim E_1$ and the short intervortex distance, the nonzero conductance stems from the CdGM mode and the MZMs. For the long intervortex distance, due to the suppression of the CdGM conductance the MZMs lead to nonzero constant conductance.

the conductance peak moves to zero, which is identical to the resonance point in the presence of the MZMs, as shown in Figs. 3(a) and 6(c). Studies [67] have shown that two separate localized fermion vortex modes can have nonzero conductance and the conductance peak located at $V_g = 0$. This tunneling stems from the thermal fluctuation of the two fermions. In the low-temperature limit ($k_B T \ll E_1, E_2$), for any intervortex distance, the gate voltage of the conductance peak is always located at E_1 unless $R \gg 1$. However, the conductance peak exponentially decreases to zero when the intervortex distance increases, as shown in Fig. 6(b). The reason is that when the tunneling of the thermal fluctuation for the localized fermions is suppressed, the conductance is approximately proportional to $e^{-2R/\xi}$ due to the exponential wave-function decay of the CdGM mode.

(b) While each vortex possesses an MZM, the left vortex traps an additional CdGM mode with energy E_1 . On the one hand, the tunneling rates of the CdGM mode are identical to those of case (a) ($\Gamma_1^l = \Lambda_1^l = 1$ and $\Gamma_1^r = \Lambda_1^r = e^{-2R/\xi}$). On the other hand, we consider that the MZM wave functions $\Phi_l(r)$ and $\Phi_r(r)$ are located on the left and right vortices, respectively. With the spatial exponential decay, $|\Phi_l(r_l)| \gg |\Phi_l(r_r)|$ and $|\Phi_r(r_r)| \gg |\Phi_r(r_l)|$, where r_l and r_r are the locations of the left and right vortices. Since the two MZMs form a fermion with $E_2 = 0$ and the tunneling rates of this fermion state at the two different vortex cores are proportional to $|\Phi_l(r_l)|^2$ and $|\Phi_r(r_r)|^2$ separately, the tunneling rates are independent of the intervortex distance R . Therefore, without loss of generality, we can assume for the tunneling rates of the MZMs that $\Gamma_2^r = \Lambda_2^r = \Gamma_2^l = \Lambda_2^l = 1$. Similarly, the conductance as a

function of V_g is computed at $T = 0.1 \text{ meV} \sim E_1, E_2$ and $T = 0.01 \text{ meV} \ll E_1, E_2$. In the presence of the MZMs trapped by the two vortices, the conductance peak behaves differently from the vortices without MZMs. At any temperature, the gate voltage of the conductance peak is located at zero and the conductance is never suppressed in any circumstances due to the resonant tunneling via the MZMs [72]. In other words, the tunneling rates at the two terminals are nonzero. For $k_B T \sim E_1$, the CdGM mode contributes a small portion of the conductance peak in the short intervortex distance, as shown in Figs. 3(b) and 6(d). As the intervortex distance increases, the CdGM contribution is suppressed and the conductance peak is reduced and stays at a nonzero constant. On the other hand, for $k_B T \ll E_1$, the conductance peak stemming from only the resonant tunneling via MZMs is always a nonzero constant at any intervortex distance, as shown in Figs. 6(b) and 6(d).

APPENDIX D: CHARGING-ENERGY ESTIMATION

The charging-energy estimation of the superconducting island is an important requirement to determine the feasibility of our readout proposal. First, the surface diameter of the island must be greater than the London penetration depth to collect enough magnetic flux for the formation of Abrikosov vortices. Second, the island has to be thick enough to avoid the coupling of the two Dirac cones on the top and bottom surfaces, since the MZMs vanish in the vortices once the Dirac cones disappear. The decay length of this cone coupling is approximately given by $v_F/\delta = 2 \text{ nm}$, where the Fermi velocity of the Dirac cone $v_F \approx 20 \text{ nm meV}$ and the bulk gap connecting the surface Dirac cone $\delta \sim 10 \text{ meV}$ [35]. However, 2 nm is not thick enough. When the thickness (d) of the superconductor is smaller than the London penetration depth of the bulk material (λ), the effective London penetration depth for the thin film depends on the thickness ($\lambda_{\text{eff}} = \lambda^2/d$) [75]. That is, a thinner SC film leads to a longer London penetration depth. Therefore, to have the localized Dirac surface and the minimum of the London penetration depth, the thickness of the SC island should be greater than the original London penetration depth (approximately 500 nm [68,69]).

We can roughly estimate the charging energy of the island by considering a sphere with radius $r = 500 \text{ nm}$:

$$E_c = \frac{e^2}{C} = \frac{e^2}{4\pi\epsilon_r\epsilon_0 r} = 2.9 \text{ meV}, \quad (\text{D1})$$

where we use $\epsilon_r = 1$ in the estimation. However, since the substrate always possesses a relative permittivity ϵ_r greater than one, the charging energy of the island is commonly less than 2.9 meV.

- [1] N. Read and Dmitry Green, Paired states of fermions in two dimensions with breaking of parity and time-reversal symmetries and the fractional quantum Hall effect, *Phys. Rev. B* **61**, 10267 (2000).
- [2] A. Yu Kitaev, Unpaired Majorana fermions in quantum wires, *Phys. Usp.* **44**, 131 (2001).
- [3] Chetan Nayak, Steven H. Simon, Ady Stern, Michael Freedman, and Sankar Das Sarma, Non-Abelian anyons and topological quantum computation, *Rev. Mod. Phys.* **80**, 1083 (2008).
- [4] Jason Alicea, New directions in the pursuit of Majorana fermions in solid state systems, *Rep. Prog. Phys.* **75**, 076501 (2012).
- [5] Martin Leijnse and Karsten Flensberg, Introduction to topological superconductivity and Majorana fermions, *Semicond. Sci. Technol.* **27**, 124003 (2012).
- [6] C. W. J. Beenakker, Search for Majorana fermions in superconductors, *Annu. Rev. Condens. Matter Phys.* **4**, 113 (2013).
- [7] Tudor D. Stanescu and Sumanta Tewari, Majorana fermions in semiconductor nanowires: Fundamentals, modeling, and experiment, *J. Phys.: Condens. Matter* **25**, 233201 (2013).
- [8] Jian-Hua Jiang and Si Wu, Non-Abelian topological superconductors from topological semimetals and related systems under the superconducting proximity effect, *J. Phys.: Condens. Matter* **25**, 055701 (2013).
- [9] Sankar Das Sarma, Michael Freedman, and Chetan Nayak, Majorana zero modes and topological quantum computation, *npj Quantum Inf.* **1**, 15001 EP (2015).
- [10] Steven R. Elliott and Marcel Franz, Colloquium: Majorana fermions in nuclear, particle, and solid-state physics, *Rev. Mod. Phys.* **87**, 137 (2015).
- [11] Masatoshi Sato and Satoshi Fujimoto, Majorana fermions and topology in superconductors, *J. Phys. Soc. Jpn.* **85**, 072001 (2016).
- [12] Masatoshi Sato and Yoichi Ando, Topological superconductors: A review, *Rep. Prog. Phys.* **80**, 076501 (2017).
- [13] R. Aguado, Majorana quasiparticles in condensed matter, *Riv. Nuovo Cimento* **40**, 523 (2017).
- [14] R. M. Lutchyn, E. P. A. M. Bakkers, L. P. Kouwenhoven, P. Krogstrup, C. M. Marcus, and Y. Oreg, Majorana zero modes in superconductor-semiconductor heterostructures, *Nat. Rev. Mater.* **3**, 52 (2018).
- [15] A. Yu Kitaev, Fault-tolerant quantum computation by anyons, *Ann. Phys.* **303**, 2 (2003).
- [16] D. A. Ivanov, Non-Abelian Statistics of Half-Quantum Vortices in p -Wave Superconductors, *Phys. Rev. Lett.* **86**, 268 (2001).
- [17] Liang Fu and C. L. Kane, Superconducting Proximity Effect and Majorana Fermions at the Surface of a Topological Insulator, *Phys. Rev. Lett.* **100**, 096407 (2008).
- [18] Jay D. Sau, Roman M. Lutchyn, Sumanta Tewari, and S. Das Sarma, Generic New Platform for Topological Quantum Computation Using Semiconductor Heterostructures, *Phys. Rev. Lett.* **104**, 040502 (2010).
- [19] Roman M. Lutchyn, Jay D. Sau, and S. Das Sarma, Majorana Fermions and a Topological Phase Transition

- in Semiconductor-Superconductor Heterostructures, *Phys. Rev. Lett.* **105**, 077001 (2010).
- [20] Yuval Oreg, Gil Refael, and Felix von Oppen, Helical Liquids and Majorana Bound States in Quantum Wires, *Phys. Rev. Lett.* **105**, 177002 (2010).
- [21] Rui-Xing Zhang, William S. Cole, and S. Das Sarma, Helical Hinge Majoranas in Iron-Based Superconductors, *Phys. Rev. Lett.* **122**, 187001 (2019).
- [22] V. Mourik, K. Zuo, S. M. Frolov, S. R. Plissard, E. P. A. M. Bakkers, and L. P. Kouwenhoven, Signatures of Majorana fermions in hybrid superconductor-semiconductor nanowire devices, *Science* **336**, 1003 (2012).
- [23] Leonid P. Rokhinson, Xinyu Liu, and Jacek K. Furdyna, The fractional ac Josephson effect in a semiconductor-superconductor nanowire as a signature of Majorana particles, *Nat. Phys.* **8**, 795 (2012).
- [24] M. T. Deng, C. L. Yu, G. Y. Huang, M. Larsson, P. Caroff, and H. Q. Xu, Anomalous zero-bias conductance peak in a Nb-InSb nanowire-Nb hybrid device, *Nano Lett.* **12**, 6414 (2012).
- [25] Anindya Das, Yuval Ronen, Yonatan Most, Yuval Oreg, Moty Heiblum, and Hadas Shtrikman, Zero-bias peaks and splitting in an Al-InAs nanowire topological superconductor as a signature of Majorana fermions, *Nat. Phys.* **8**, 887 (2012).
- [26] H. O. H. Churchill, V. Fatemi, K. Grove-Rasmussen, M. T. Deng, P. Caroff, H. Q. Xu, and C. M. Marcus, Superconductor-nanowire devices from tunneling to the multichannel regime: Zero-bias oscillations and magnetoconductance crossover, *Phys. Rev. B* **87**, 241401 (2013).
- [27] A. D. K. Finck, D. J. Van Harlingen, P. K. Mohseni, K. Jung, and X. Li, Anomalous Modulation of a Zero-Bias Peak in a Hybrid Nanowire-Superconductor Device, *Phys. Rev. Lett.* **110**, 126406 (2013).
- [28] S. Nadj-Perge, I. K. Drozdov, J. Li, H. Chen, S. Jeon, J. Seo, A. H. MacDonald, B. A. Bernevig, and A. Yazdani, Observation of Majorana fermions in ferromagnetic atomic chains on a superconductor, *Science* **346**, 602 (2014).
- [29] S. M. Albrecht, A. P. Higginbotham, M. Madsen, F. Kuemmeth, T. S. Jespersen, Jesper Nygård, P. Krogstrup, and C. M. Marcus, Exponential protection of zero modes in Majorana islands, *Nature* **531**, 206 (2016).
- [30] M. T. Deng, S. Vaitiekenas, E. B. Hansen, J. Danon, M. Leijnse, K. Flensberg, J. Nygård, P. Krogstrup, and C. M. Marcus, Majorana bound state in a coupled quantum-dot hybrid-nanowire system, *Science* **354**, 1557 (2016).
- [31] Hao Zhang *et al.*, Ballistic superconductivity in semiconductor nanowires, *Nat. Commun.* **8**, 16025 EP (2017).
- [32] Hao Zhang *et al.*, Quantized Majorana conductance, *Nature* **556**, 74 (2018).
- [33] Jin-Peng Xu, Mei-Xiao Wang, Zhi Long Liu, Jian-Feng Ge, Xiaojun Yang, Canhua Liu, Zhu An Xu, Dandan Guan, Chun Lei Gao, Dong Qian, Ying Liu, Qiang-Hua Wang, Fu-Chun Zhang, Qi-Kun Xue, and Jin-Feng Jia, Experimental Detection of a Majorana Mode in the Core of a Magnetic Vortex Inside a Topological Insulator-Superconductor $\text{Bi}_2\text{Te}_3/\text{NbSe}_2$ Heterostructure, *Phys. Rev. Lett.* **114**, 017001 (2015).
- [34] Hao-Hua Sun, Kai-Wen Zhang, Lun-Hui Hu, Chuang Li, Guan-Yong Wang, Hai-Yang Ma, Zhu-An Xu, Chun-Lei Gao, Dan-Dan Guan, Yao-Yi Li, Canhua Liu, Dong Qian, Yi Zhou, Liang Fu, Shao-Chun Li, Fu-Chun Zhang, and Jin-Feng Jia, Majorana Zero Mode Detected with Spin Selective Andreev Reflection in the Vortex of a Topological Superconductor, *Phys. Rev. Lett.* **116**, 257003 (2016).
- [35] Dongfei Wang, Lingyuan Kong, Peng Fan, Hui Chen, Shiyu Zhu, Wenyao Liu, Lu Cao, Yujie Sun, Shixuan Du, John Schneeloch, Ruidan Zhong, Genda Gu, Liang Fu, Hong Ding, and Hong-Jun Gao, Evidence for Majorana bound states in an iron-based superconductor, *Science* **362**, 333 (2018).
- [36] Peng Zhang, Koichiro Yaji, Takahiro Hashimoto, Yuichi Ota, Takeshi Kondo, Kozo Okazaki, Zhijun Wang, Jinsheng Wen, G. D. Gu, Hong Ding, and Shik Shin, Observation of topological superconductivity on the surface of an iron-based superconductor, *Science* **360**, 182 (2018).
- [37] T. Machida, Y. Sun, S. Pyon, S. Takeda, Y. Kohsaka, T. Hanaguri, T. Sasagawa, and T. Tamegai, Zero-energy vortex bound state in the superconducting topological surface state of $\text{Fe}(\text{Se},\text{Te})$, *Nat. Mater.* **18**, 1 (2019).
- [38] Qin Liu, Chen Chen, Tong Zhang, Rui Peng, Ya-Jun Yan, Chen-Hao-Ping Wen, Xia Lou, Yu-Long Huang, Jin-Peng Tian, Xiao-Li Dong, Guang-Wei Wang, Wei-Cheng Bao, Qiang-Hua Wang, Zhi-Ping Yin, Zhong-Xian Zhao, and Dong-Lai Feng, Robust and Clean Majorana Zero Mode in the Vortex Core of High-Temperature Superconductor $(\text{Li}_{0.84}\text{Fe}_{0.16})\text{OHFeSe}$, *Phys. Rev. X* **8**, 041056 (2018).
- [39] Mason J. Gray, Josef Freudenstein, Shu Yang F. Zhao, Ryan O'Connor, Samuel Jenkins, Narendra Kumar, Marcel Hoek, Abigail Kopec, Takashi Taniguchi, Kenji Watanabe, *et al.*, Evidence for helical hinge zero modes in an Fe-based superconductor, arXiv:1902.10723 (2019).
- [40] Zhenyu Wang, Jorge Olivares Rodriguez, Martin Graham, G. D. Gu, Taylor Hughes, Dirk K. Morr, and Vidya Madhavan, Signature of dispersing 1D Majorana channels in an iron-based superconductor, arXiv:1903.00515 (2019).
- [41] K. T. Law, Patrick A. Lee, and T. K. Ng, Majorana Fermion Induced Resonant Andreev Reflection, *Phys. Rev. Lett.* **103**, 237001 (2009).
- [42] Lun-Hui Hu, Chuang Li, Dong-Hui Xu, Yi Zhou, and Fu-Chun Zhang, Theory of spin-selective Andreev reflection in the vortex core of a topological superconductor, *Phys. Rev. B* **94**, 224501 (2016).
- [43] C. Caroli, P. G. De Gennes, and J. Matricon, Bound fermion states on a vortex line in a type II superconductor, *Phys. Lett.* **9**, 307 (1964).
- [44] Shiyu Zhu, Lingyuan Kong, Lu Cao, Hui Chen, Shixuan Du, Yuqing Xing, Wenyao Liu, Dongfei Wang, Chengmin Shen, Fazhi Yang, John Schneeloch, Ruidan Zhong, Genda Gu, Liang Fu, Yu-Yang Zhang, Hong Ding, and Hong-Jun Gao, Observation of Majorana conductance plateau by scanning tunneling spectroscopy, arXiv:1904.06124 (2019).
- [45] C. Chen, Q. Liu, T. Z. Zhang, D. Li, P. P. Shen, X. L. Dong, Z.-X. Zhao, T. Zhang, and D. L. Feng, Quantized conductance of Majorana zero mode in the vortex of the topological superconductor $(\text{Li}_{0.84}\text{Fe}_{0.16})\text{OHFeSe}$, *Chin. Phys. Lett.* **36**, 057403 (2019).
- [46] Liang Fu, Electron Teleportation via Majorana Bound States in a Mesoscopic Superconductor, *Phys. Rev. Lett.* **104**, 056402 (2010).

- [47] Stephan Plugge, Asbjørn Rasmussen, Reinhold Egger, and Karsten Flensberg, Majorana box qubits, *New J. Phys.* **19**, 012001 (2017).
- [48] Torsten Karzig, Christina Knapp, Roman M. Lutchyn, Parsa Bonderson, Matthew B. Hastings, Chetan Nayak, Jason Alicea, Karsten Flensberg, Stephan Plugge, Yuval Oreg, Charles M. Marcus, and Michael H. Freedman, Scalable designs for quasiparticle-poisoning-protected topological quantum computation with Majorana zero modes, *Phys. Rev. B* **95**, 235305 (2017).
- [49] Dmitry Pikulin, Karsten Flensberg, Leonid I. Glazman, Manuel Houzet, and Roman M. Lutchyn, Coulomb Blockade of a Nearly Open Majorana Island, *Phys. Rev. Lett.* **122**, 016801 (2019).
- [50] Meng Cheng, Roman M. Lutchyn, Victor Galitski, and S. Das Sarma, Splitting of Majorana-Fermion Modes due to Intervortex Tunneling in a $p_x + ip_y$ Superconductor, *Phys. Rev. Lett.* **103**, 107001 (2009).
- [51] Meng Cheng, Roman M. Lutchyn, Victor Galitski, and S. Das Sarma, Tunneling of anyonic Majorana excitations in topological superconductors, *Phys. Rev. B* **82**, 094504 (2010).
- [52] Tom Dvir, Marco Aprili, Charis H. L. Quay, and Hadar Steinberg, Tunneling into the vortex state of nbse2 with van der waals junctions, *Nano Lett.* **18**, 7845 (2018).
- [53] T. Dvir, F. Masee, L. Attias, M. Khodas, M. Aprili, C. H. L. Quay, and H. Steinberg, Spectroscopy of bulk and few-layer superconducting NbSe₂ with van der Waals tunnel junctions, *Nat. Commun.* **9**, 598 (2018).
- [54] Yuan Pang, Jie Shen, Junhua Wang, Junya Feng, Fanming Quu, Zhaozhen Lyu, Jie Fan, Guangtong Li, Zhongqing Ji, and Xiunian Jing, *et al.*, Majorana fermions in a superconducting Möbius strip, arXiv:1503.00838 (2015).
- [55] Xiaoxiang Xi, Zefang Wang, Weiwei Zhao, Ju-Hyun Park, Kam Tuen Law, Helmuth Berger, László Forró, Jie Shan, and Kin Fai Mak, Ising pairing in superconducting NbSe₂ atomic layers, *Nat. Phys.* **12**, 139 EP (2015).
- [56] Jian-Feng Ge, Zhi-Long Liu, Chun-Lei Gao, Dong Qian, Canhua Liu, and Jin-Feng Jia, Development of micro-four-point probe in a scanning tunneling microscope for *in situ* electrical transport measurement, *Rev. Sci. Instrum.* **86**, 053903 (2015).
- [57] O. Kubo, Y. Shingaya, M. Nakaya, M. Aono, and T. Nakayama, Epitaxially grown WO_x nanorod probes for sub-100 nm multiple-scanning-probe measurement, *Appl. Phys. Lett.* **88**, 254101 (2006).
- [58] E. W. J. Straver, J. E. Hoffman, O. M. Auslaender, D. Rugar, and Kathryn A. Moler, Controlled manipulation of individual vortices in a superconductor, *Appl. Phys. Lett.* **93**, 172514 (2008).
- [59] Benjamin H. November, Jay D. Sau, James R. Williams, and Jennifer E. Hoffman, Scheme for Majorana manipulation using magnetic force microscopy, arXiv:1905.09792 (2019).
- [60] Ching-Kai Chiu, T. Machida, Yingyi Huang, T. Hanaguri, and Fu-Chun Zhang, Scalable Majorana vortex modes in iron-based superconductors, arXiv:1904.13374 (2019).
- [61] Mingyang Chen, Xiaoyu Chen, Huan Yang, Zengyi Du, Xiyu Zhu, Enyu Wang, and Hai-Hu Wen, Discrete energy levels of Caroli–de Gennes–Matricon states in quantum limit in FeTe_{0.55}Se_{0.45}, *Nat. Commun.* **9**, 970 (2018).
- [62] Lingyuan Kong, Shiyu Zhu, Michał Papaj, Lu Cao, Hiroki Isobe, Wenyao Liu, Dongfei Wang, Peng Fan, Hui Chen, Yujie Sun *et al.*, Observation of half-integer level shift of vortex bound states in an iron-based superconductor, *Nat. Phys.* **15**, 1181 (2019).
- [63] T. Machida, Y. Kohsaka, and T. Hanaguri, A scanning tunneling microscope for spectroscopic imaging below 90 mK in magnetic fields up to 17.5 T, *Rev. Sci. Instrum.* **89**, 093707 (2018).
- [64] Parsa Bonderson, Michael Freedman, and Chetan Nayak, Measurement-Only Topological Quantum Computation, *Phys. Rev. Lett.* **101**, 010501 (2008).
- [65] Sagar Vijay and Liang Fu, Teleportation-based quantum information processing with Majorana zero modes, *Phys. Rev. B* **94**, 235446 (2016).
- [66] B. van Heck, R. M. Lutchyn, and L. I. Glazman, Conductance of a proximitized nanowire in the Coulomb blockade regime, *Phys. Rev. B* **93**, 235431 (2016).
- [67] Ching-Kai Chiu, Jay D. Sau, and S. Das Sarma, Conductance of a superconducting Coulomb-blockaded Majorana nanowire, *Phys. Rev. B* **96**, 054504 (2017).
- [68] H. Kim, C. Martin, R. T. Gordon, M. A. Tanatar, J. Hu, B. Qian, Z. Q. Mao, Rongwei Hu, C. Petrovic, N. Salovich, R. Giannetta, and R. Prozorov, London penetration depth and superfluid density of single-crystalline Fe_{1+y}(Te_{1-x}Se_x) and Fe_{1+y}(Te_{1-x}S_x), *Phys. Rev. B* **81**, 180503 (2010).
- [69] T. Klein, D. Braithwaite, A. Demuer, W. Knafo, G. Laperot, C. Marcenat, P. Rodière, I. Sheikin, P. Strobel, A. Sulpice, and P. Toulemonde, Thermodynamic phase diagram of Fe(Se_{0.5}Te_{0.5}) single crystals in fields up to 28 tesla, *Phys. Rev. B* **82**, 184506 (2010).
- [70] Lise Serrier-Garcia, Matias Timmermans, Joris Van de Vondel, and Victor V. Moshchalkov, Pinning of superconducting vortices in MoGe/Au thin nano-squares, *Phys. C: Supercond. Appl.* **533**, 109 (2017), Ninth international conference on Vortex Matter in nanostructured Superconductors.
- [71] Tianyu Liu and M. Franz, Electronic structure of topological superconductors in the presence of a vortex lattice, *Phys. Rev. B* **92**, 134519 (2015).
- [72] Liang Fu, Electron Teleportation via Majorana Bound States in a Mesoscopic Superconductor, *Phys. Rev. Lett.* **104**, 056402 (2010).
- [73] N. Hayashi, T. Isoshima, M. Ichioka, and K. Machida, Low-Lying Quasiparticle Excitations Around a Vortex Core in Quantum Limit, *Phys. Rev. Lett.* **80**, 2921 (1998).
- [74] Takuto Kawakami and Xiao Hu, Evolution of Density of States and a Spin-Resolved Checkerboard-Type Pattern Associated with the Majorana Bound State, *Phys. Rev. Lett.* **115**, 177001 (2015).
- [75] P. G. de Gennes, *Superconductivity of Metals and Alloys* (Westview Press, Reading, MA, United States, 1999).